TECHNICAL ARTICLE

Friction Stir Spot Vibration Welding: Improving the Microstructure and Mechanical Properties of Al5083 Joint

Behrouz Bagheri[1] · Ali Akbar Mahdian Rizi[2] · Mahmoud Abbasi[2] · Mohammad Givi[2]

Abstract

In this study, a modified version of friction stir spot welding (FSSW) is applied to join Al5083 specimens. In respect to conventional FSSW, this new method leads to better characteristics, finer grain sizes in the stir zone and higher mechanical properties. In this method, the workpiece is vibrated normal to tool axis direction during FSSW. This process is entitled friction stir spot vibration welding (FSSVW). The finite element method (FEM) was used to validate the experimental results. The FEM and experimental results had a good agreement. The microstructure of the welded zone was analyzed by scanning electron microscopy and optical microscopy. The results showed that the presence of vibration during FSSW led to more grain refinement. This was related to more straining of material in the welded zone which enhanced the dynamic recovery and recrystallization and increased the grain refinement. The results showed that grain size of welded region for friction stir spot-welded specimen was about 35% lower than that for friction stir spot-welded specimen. Mechanical properties such as tensile shear load and hardness increased as the vibration was applied. Also, mechanical properties increased as vibration frequency increased from 28 to 38 Hz during FSSVW.

Abbreviations

FSSW	Friction stir spot welding
FSSVW	Friction stir spot vibration welding
S-FSSVW	Simulation of friction stir spot welding
HAZ	Heat-affected zone
TMAZ	Thermo-mechanical-affected zone
WNZ	Weld nugget zone
UAFSW	Ultrasonic-assisted friction stir welding
SEM	Scanning electron microscopy
CEL	Coupled Eulerian–Lagrangian
JCP	Johnson–Cook plasticity
EDS	Energy-dispersive spectrometry

List of Symbols

Z	Zener–Hollomon parameter
R	Gas constant
σ	Static yield stress
ε	Equivalent plastic strain

✉ Behrouz Bagheri
b.bagheri@aut.ac.ir; b.bagheripersian@yahoo.com

[1] Department of Mining and Metallurgy, Amirkabir University of Technology, Tehran, Iran

[2] Faculty of Engineering, University of Kashan, Kashan, Iran

Introduction

Friction stir spot welding (FSSW) is a solid-state joining process in which the base metal is not melted during welding. Like the FSW, the process begins by entering a rotating tool into the workpiece. This process consists of three steps: plunging, stirring and drawing out. Based on Fig. 1, during the plunging step, the tool penetrates into the workpiece, and due to friction between the tool and the workpiece, a high amount of heat is produced. As the temperature of the workpiece increases, the weldment material near the FSSW tool becomes soft and it can flow plastically easily. Once the tool reaches the desired level of penetration into the workpiece, the plunge motion of the tool is halted and the tool continues to rotate for a specified length of time (stirring step). During the "drawing-out" period, the tool comes back while the material continues to experience plastic deformation. The tool consists of two parts: the shoulder and a pin. Shoulder contacts the metal surfaces while pin penetrates

Fig. 1 Schematic view of FSSW and its steps

Plunging   Stirring   Drawing out
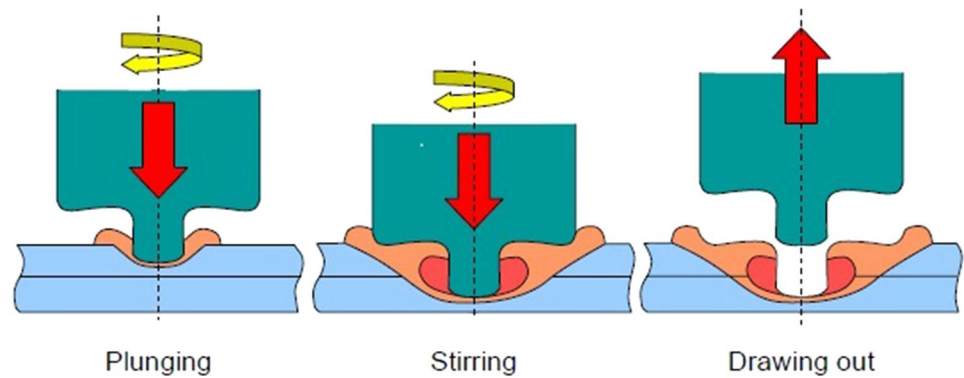
into the workpiece. The distance the tool's pin penetrates into the workpiece during welding is defined as the "heel plunge depth" or "plunge depth." The time the tool remains plunged in the workpiece is defined as the "dwell time." The velocity at which the tool plunges into the workpiece is defined as the "plunge rate," and the velocity at which the tool is withdrawn from the weld is defined as the "extraction rate."

FSSW has desirable characteristics, and it has been applied to join different materials, especially aluminum alloys. So, it is necessary to identify the effect of FSSW parameters on the weld performance [1–4]. Mechanical properties of the weld produced between AA6082-T6 sheets via FSSW were investigated by Tuncel et al. [5]. The results showed that the tensile shear load increased almost linearly with increasing plunge depth. Srinivasulu and Mehta [6] investigated the various shapes of EN19 and EN 31 profile tool in FSSW process of AA6082 sheets. They found that the EN31 taper thread tool provided better results rather than that of other tool shapes. Srirangarajalu [7] studied the FSSW of AA1100 sheets with a thickness of 3 mm using a 5.9 mm pin length. He indicated that the stir zone hardness was high due to recrystallization of the material. The effects of FSSW parameters on tensile shear strength of friction stir spot (FSS)-welded lap joint between AA5005 alloys were determined by Kulekci [8]. The results showed that the weld performance was significantly affected by the tool rotation, dwell time and the tool pin height.

Toshiya et al. [9] investigated the high-temperature deformation during FSSW for aluminum sheets. According to results, the maximum temperature decreased from 450 to 289 °C as rotation speed decreased from 1000 rpm to 500 rpm. The effect of shoulder size on microstructure of joint made by FSSW between galvanized BH plates was studied by Sheikhhasani et al. [10]. They found that grain size decreased by 23% in SZ and 15% in TMAZ by increasing shoulder diameter from 10 to 14 mm. Wook Baek et al. [11] investigated the microstructure and mechanical properties of joints made by FSSW for galvanized steels. They reported that the tensile shear strength of the joint increased

to a maximum value of 3.07 kN at a tool penetration depth of 0.52 mm. Aghdam et al. [12] studied the correlation between natural frequencies and fatigue crack initiation of the FSSW in four different welding processes. Fatigue and experimental modal analysis tests, as well as finite element modeling using Abaqus software, were done at different fatigue strength levels. They found good agreement between the FE model and experimental test results. Dey et al. [13] determined the mechanical properties of aluminum alloys during FSSW. Their results indicated that the average hardness value of the nugget zone was significantly lower than that of the base alloy.

Various trials have been implemented to improve FSSW and to get better characteristics for the weld. Some of these trails were done to eliminate the keyhole in the weld region, and some were implemented to improve the characteristics of the joint. Helmholtz-Zentrum Geesthacht [14] patented the refill FSSW process as a method to fill the keyhole and to obtain a high strength weld. This method consists of four steps including friction, first extrusion, second extrusion and pull out, and the tool has three parts, namely pin, sleeve and clamp. This method led to a flat surface joint with minimum material loss. Sun et al. [15] used a two-step FSSW technique for AA6061 and AA5052 alloys. In the first step, a specially designed backplate contained a round dent was used for conventional FSSW, and in the second step, a pinless tool and a flat backplate were applied to remove the keyhole and the protuberance. Chen et al. [16] applied an electrical current to the weld region during FSSW to decrease the welding force. They found that resistance heating induces thermal softening and a wider flow pattern and the more uniform hook is formed at the interface of Al–Fe.

Rostamiyan et al. [17] combined two welding processes: FSSW and ultrasonic welding to improve weld quality. In their method, FSSW was assisted by ultrasonic vibration of the tool. They studied the effect of process factors such as vibration, tool rotary speed, tool plunge depth and dwell time on lap shear force and hardness. They found that the presence of vibration increases the lap shear force and hardness. Ji et al. [18] introduced the

Table 1 Chemical composition of the base metal alloy (% wt)

Si	Mn	Cr	Cu	Mg	Al	Fe
0.5	0.4	0.25	0.1	4.8	Bal	0.4

"ultrasonic-assisted friction stir spot welding" (UAFSSW) method. They applied this method to weld dissimilar AZ31and AA6061alloys. They indicated that ultrasonic vibration is beneficial for the upward flow of the bottom plate and to get a sound joint. Additionally, they found that the presence of ultrasonic vibration increased the stir zone width and led to finer grains in the stir zone. Liu et al. [19] used the ultrasonic vibration of tool to enhance plastic deformation and material flow during friction stir welding. They reported that ultrasonic energy has a positive influence on the volume of deformed material, flow velocity and strain/strain rate. To improve the weld quality and weld efficiency of high melting temperature material, Park [20] utilized ultrasonic-assisted friction stir welding for Al alloy joint. He found that ultrasonic vibration of tool decreases the welding forces by 6% in peak region and about 12.5% in welding area. Ultrasonic vibration of tool was applied to improve the microstructure and mechanical properties of the 2024Al-T4 joint in friction stir welding by Liu et al. [21]. The results indicated that tensile strength, elongation of joints and the microhardness profile in the stir zone increased as ultrasonic vibration applied. Strass et al. [22] investigated the ultrasonic technology to the realization of the Al/Mg hybrid joint during friction stir welding. The results showed that the strength in UAFSW joints compared to conventional FSW could be increased up to 30%. The effect of ultrasonic vibration of tool on the friction stir welding process was studied by Amini and Amiri [23]. They found that ultrasonic vibrations can decrease the force and increase temperature, tensile strength and hardness in FSW. Ahmadnia et al. [24] considered the influence of ultrasonic vibration on mechanical and microstructure behaviors of AA6061 joints during FSW. The results indicated that ultrasonic had an important effect on welding process and the joints fabricated at 400WUS power, 1000 RPM tool rotary speed, 40 mm/min traverse speed and 8 kN axial force had higher mechanical properties than other joints. Liu et al. [25] applied ultrasonic vibration of tool during FSW to join Mg and Al alloys. They found that UAFSW had the potential to join Al/Mg alloys.

The problem in regard to UAFSW and UAFSSW is the high cost of equipment, namely the ultrasonic generator and transducer, and its application is not easy. In the current research, unlike conventional UAFSW, in which the tool is vibrated by ultrasonic, the workpiece is vibrated mechanically in a direction normal to the tool axis direction. This new method is called friction stir spot vibration

Table 2 Mechanical properties of the base metal alloy

Ys, MPa	UTS, MPa	Elongation, %	E, GPa	Hardness, V
184	307	15	71	94

welding (FSSVW). The finite element method (FEM) was applied to validate the experimental results.

Materials and Methods

Experimental Work

In the current research, AA5083 aluminum sheets with 2 and 0.7 mm thicknesses were used as base metals and joining specimens. The chemical composition and mechanical properties of the base metal are listed in Tables 1 and 2, respectively.
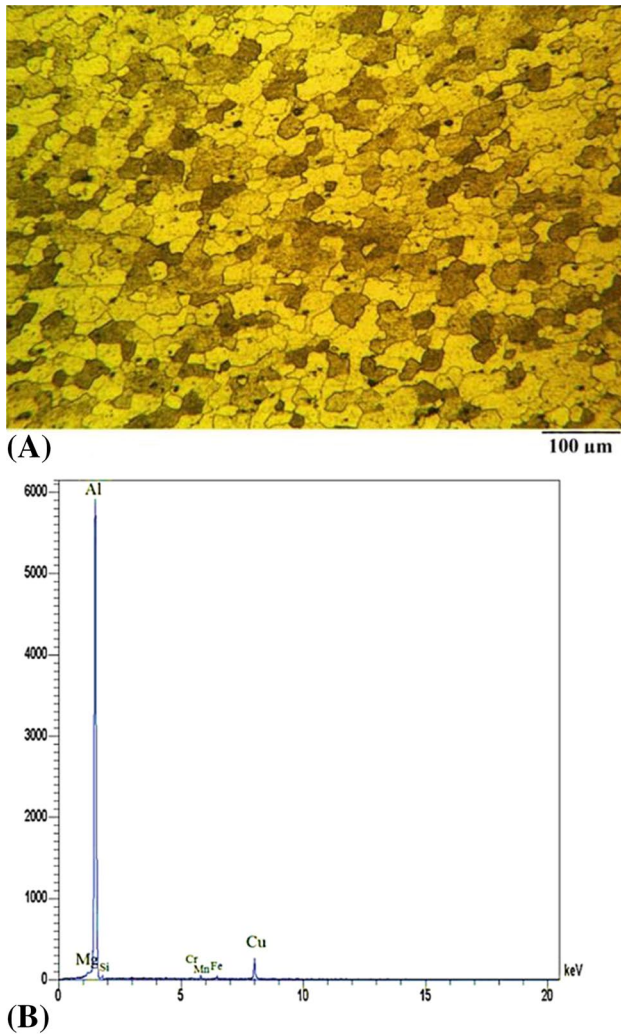
Microstructure and energy-dispersive spectrometry (EDS) curve of the studied material are presented in Fig. 2. Samples were cut into pieces in dimensions of 100 mm length and 25 mm width, and these pieces were FSS welded in the overlapping configuration while overlapping distance was 25 mm.

Both FSSW and FSSVW were carried out by milling machine. For FSSVW, a special machine is designed and manufactured. Figure 3 shows the schematic design of FSSVW machine. Based on Fig. 3, the vibration is applied through fixture and rotation movement of the motor shaft is transformed to linear motion of fixture using a camshaft. The fixture is mounted on the sliding plate, and the specimen is fixed on it. The camshaft is designed as the vibration amplitude for the sliding plate is 0.5 mm. The motor is equipped by a driver to get different vibration frequencies. The welding parameters used in this research are presented in Table 3.

Figure 4 shows the geometry of the tool used for FSSW and FSSVW processes. A two-piece tool which consisted of a shoulder from M2 steel and a pin from carbide tungsten was utilized for the process. Shoulder with the hardness of 65 HRC had good durability to wear and heat.

The strength of the welds was evaluated by tensile shear tests. The shape of the test pieces used in the tensile shear tests is shown in Fig. 5. Tensile shear tests were performed at room temperature with a crosshead speed of 0.5 mm/min.

FSS-welded specimens were cross-sectioned normal to the processing line to analyze the microstructure. Metallography was carried out according to ASTM-E3-11 [26]. The grain size was determined by the application of the linear

Fig. 2 (**a**) Microstructure and (**b**) energy-dispersive spectrometry of the studied aluminum

intercept method based on ASTM-E112 [27] standard test. Hardness was investigated using a Vickers hardness test (HV) method. Microhardness tests were performed on polished samples using a programmable hardness test machine.

Finite Element Analysis

FSSW and FSSVW processes were modeled by Abaqus/Explicit software to do a mechanical analysis. As it is shown in Fig. 6, different mesh element sizes were assigned to different regions. In this study, welding processes were modeled as three-dimensional by using CAX4R elements [28]. Coulomb friction law was considered between contacting surfaces of tool and workpieces, and 0.35 was applied as friction coefficient. The initial temperature was assumed to be 25 °C, and also 100% of the dissipated energy caused by friction was assumed to be transformed into heat. In

these simulations, the Coupled Eulerian–Lagrangian (CEL) method was performed. In a CEL analysis, bodies that undergo large deformations are meshed with Eulerian elements, while stiffer bodies in the model are meshed with more efficient Lagrangian elements.

The Johnson–Cook plasticity equations (JCP) were used to model the behavior of materials during welding processes:

$$\overline{\sigma} = \left[A + B\left(\overline{\varepsilon}^{\mathrm{pl}} \right)^n \right] \left\{ 1 + C\mathrm{Ln}\left(\frac{\dot{\varepsilon}^{\mathrm{pl}}}{\dot{\varepsilon}_0} \right) \right\} \left(1 - \widehat{\theta}^{m} \right) \qquad (1)$$

where $\dot{\varepsilon}^{\mathrm{pl}}, \overline{\varepsilon}^{\mathrm{pl}}, \overline{\sigma}$ are the equivalent plastic strain rate, the equivalent plastic strain and yield stress, respectively. In Eq 1, A, B, C, m, n and $\dot{\varepsilon}_0$ are constants, and $\widehat{\theta}$ is a dimensionless factor used to include the effect of temperature, as indicated by:

$$\widehat{\theta} = \begin{cases} 0 & \theta < \theta_{\mathrm{transition}} \\ \left(\frac{\theta - \theta_{\mathrm{transition}}}{\theta_{\mathrm{melt}} - \theta_{\mathrm{transition}}} \right) & \theta_{\mathrm{transition}} \le \theta \le \theta_{\mathrm{melt}} \\ 1 & \theta > \theta_{\mathrm{melt}} \end{cases} \qquad (2)$$

In Eq 2, θ, θmelt and θtransition are the instantaneous temperature, melting point and the transfer temperatures, respectively. The Johnson–Cook parameters for the studied material were determined based on Ref. [29], and they are presented in Table 4.

Theoretical Method for Heat Generation

The heat generated in welding is a result of intimate contact between the tool and workpiece. The relationship between the heat generated and the process is complex and depends on different factors such as welding tool geometry, process parameters, the workpiece and tool materials, and workpiece deformation. The power input into the weld can be determined using the rotational speed of the tool and the weld torque [30, 31]:

$$P = M \times \omega \qquad (3)$$

where P is the welding power (W), M is the weld torque (N m) and ω is the tool's angular velocity (rad/s). The majority of this heat is transferred into the workpiece, and the rest is lost to the welding environment. The heat transferred into the workpiece (Qtotal) is given by [32]:

$$Q_{\mathrm{total}} = \eta P, \ 0 \prec \eta \prec 1 \qquad (4)$$

Values of η can be determined by inverse modeling [33]. As it is mentioned, the amount of heat generated by the tool depends on the surface contact area between the welding tool and workpiece; therefore,

$$\mathrm{d}Q_{\mathrm{total}} = \omega \mathrm{d}M = \omega r \mathrm{d}F = \omega r \tau_{\mathrm{contact}} \mathrm{d}A \qquad (5)$$

where dF, r and dA are an infinitesimal force, segment and area, respectively, and τcontact is the contact shear stress

Fig. 3 Schematic view of machine used for FSSVW process
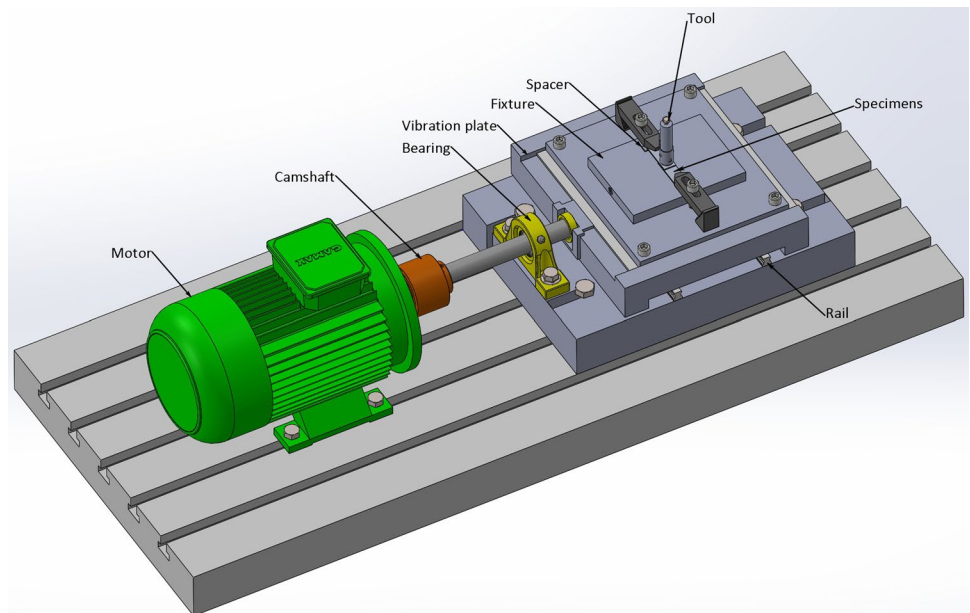
Table 3 Welding parameters values for various welding conditions

| Sample no.	Rotational speed, rpm	Dwell time, s	Vibration frequencies, Hz
1	1500	5	28
2	1500	5	38
3	1500	10	28
4	1500	10	38

within the weldment. Integrating Eq 5 for a simple flat shoulder, without pin, gives:

$$Q_{total} = \frac{2}{3}\pi\omega\tau_{contact}R^3 \tag{6}$$
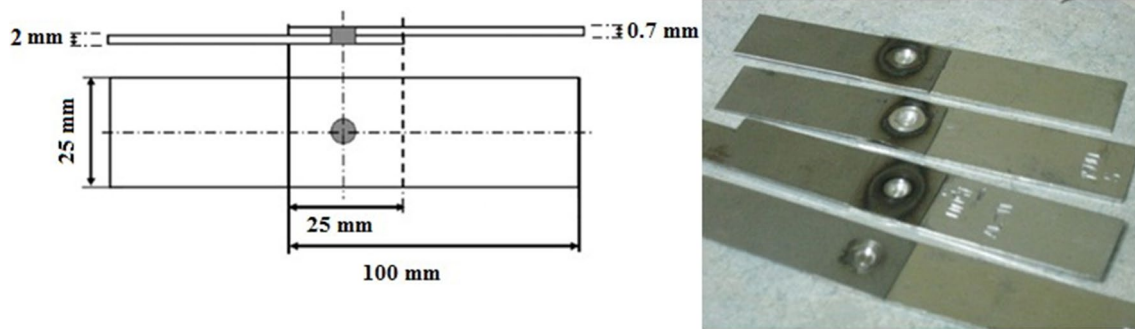
where R is the radius (m) of the shoulder. The total amount of heat generated during welding is presented as [33, 34]:

$$Q_{total} = (1 - \delta)Q_{Friction} + \delta Q_{Deformation} \tag{7}$$

where δ represents the dimensionless contact state variable at the shoulder surface. The amount of heat generated by
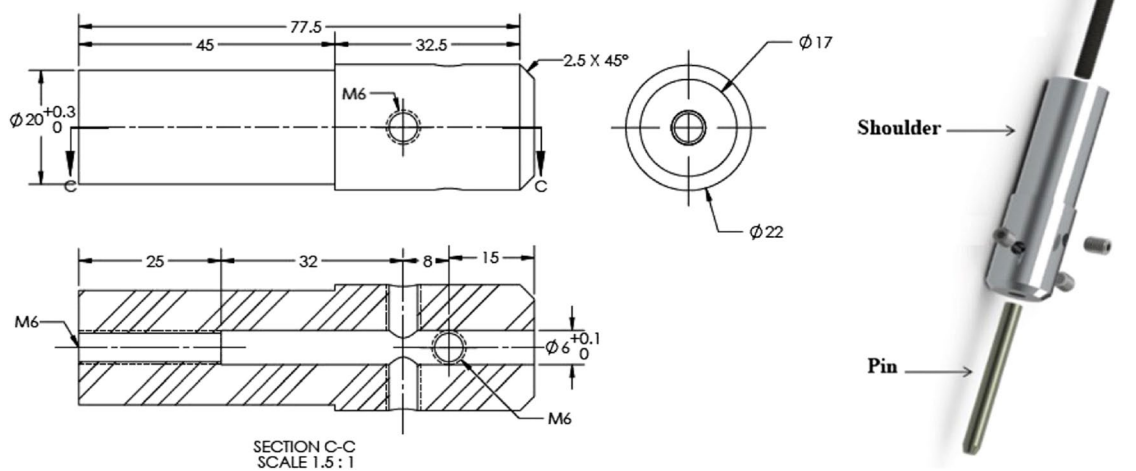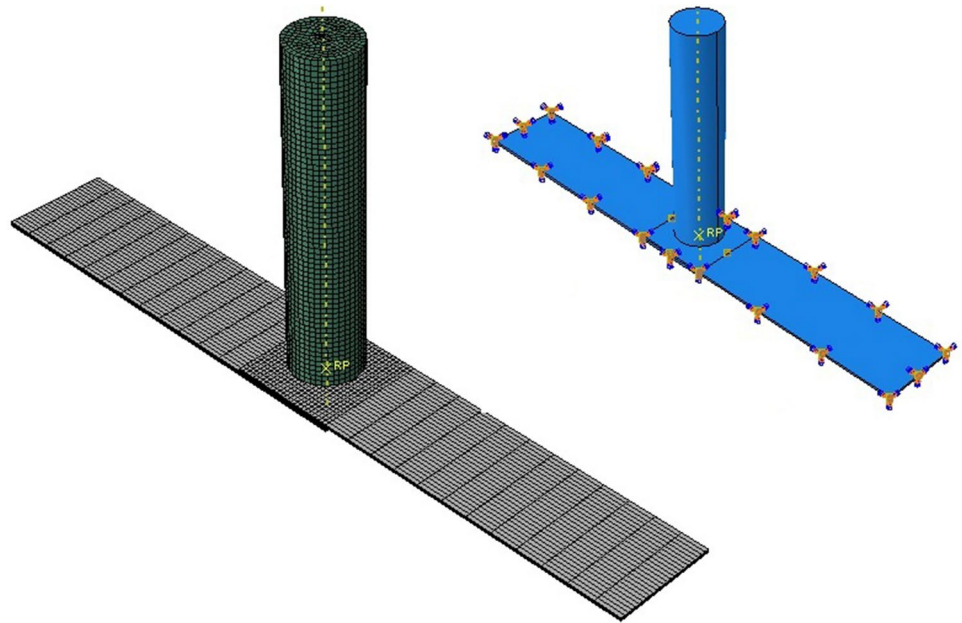

Fig. 4 Welding tool used in this study (all dimensions are in mm)

Fig. 5 Configuration of the specimens used for the tensile shear test

Fig. 6 Schematic view of finite element modeling used for FSSW and FSSVW

Table 4 Johnson–Cook equation parameters of the base metal alloy [22]

A, MPa	B, MPa	n	m	Melting temp, °K	Transition temp, °K	Strain rate coefficient, C	Epsilon dot zero
167	596	0.551	1	893	298	0.001	1

friction and deformation to the contact shear stress is given as:

$$\tau_{contact} = \begin{cases} \mu_f P & \text{friction - heating} \\ \tau_{yield} & \text{deformation - heating} \end{cases} \quad (8)$$

where μF is the coefficient of friction, P is the contact pressure (N/m2) and τyield is the shear yield strength of the material. The shear yield strength of a material is expressed as [35, 36]:

$$\tau_{yield} = \frac{\sigma_{yield}}{\sqrt{3}} \quad (9)$$

The coefficient of friction is often estimated to have a value about 0.3–0.4 [37]. Plastic flow is calculated with the elastic–plastic deformation equations:

$$\rho \frac{\partial^2 r_a}{\partial t^2} = \frac{\partial}{\partial x_\beta} \left(\frac{vE}{(1+v)(1-2v)} \varepsilon_{\gamma\gamma} \delta_{a\beta} + \frac{E}{(1+v)} \varepsilon_{a\beta} \right) + k_a$$

$$\varepsilon_{a\beta} = \frac{1}{2} \left(\frac{\partial u_a}{\partial x_\beta} + \frac{\partial u_\beta}{\partial x_a} \right)$$

$$(10)$$

where r_a is the coordinates of the material (m), t is the time (s), x_β is the space coordinates in Cartesian system (m), ρ is

the density (kg/m3), E is the Young modulus (Pa), v is the Poisson rate, $\varepsilon_{a\beta}$ is the strain tensor, $\delta_{\gamma\gamma}$ is the Kronecker delta, K_a is the external body force (N/m3) and u_a is the deformation vector (m). Normal stress σ^n and shear stress σ^s are obtained by Eq 11 and 12, respectively,

$$\sigma^n = \frac{E}{(1+v)}\varepsilon^n \tag{11}$$

$$\sigma^s = \frac{E}{(1+v)}\varepsilon^s. \tag{12}$$

Results and Discussion

Microstructure

Cross-sectional macrostructures of weld regions relating to FSS and friction stir spot (FSSV)-welded specimens are presented in Fig. 7. No cracks or porosities are observed in this figure which indicates that welding parameter values are fair and proper. It is observed in Fig. 7 that weld region for FSSV-welded specimen is larger than that for FSS-welded specimen. This relates to workpiece vibration during FSSW which increases the stir zone size.

The strain profiles developed in joint position during FSSW and FSSVW processes are presented in Fig. 8. Based on Fig. 8, strain values for the latter specimen are higher than those for the former one. This can be related to vibration motion of workpiece as well as stirring motion of tool which increases the material straining of material and leads to high strain values.

Microstructures of weld regions for FSS- and FSSV-welded specimens are observed in Fig. 9. Three areas including stir zone, thermo-mechanical-affected zone (TMAZ) and heat-affected zone (HAZ) are observed for each specimen. It is observed in Fig. 9 that grains in stir zones are smaller than grains in other areas and the stir zone grains in FSSV-welded specimen are smaller than those in FSS-welded specimens. It is known that that the main mechanism for grain refinement in stir zone, during FSW and FSSW processes, is the occurrence of dynamic recrystallization [38, 39].

Contact between tool and workpiece increases the temperature and softens the material around the pin and leads to severe plastic deformation [40]. As a result, high amount of dislocations are generated in specimen and dislocation density enhances. To decrease the energy level of specimen, dislocations arrange themselves in low-angle grain boundaries (LABs) with misorientation angle < 15°. As straining proceeds, the LABs transform to high-angle grain boundaries (HABs) due to dynamic recrystallization (DR) and small grains are developed within the original grains [41, 42]. In this regard, small grains develop in stir zone.

As workpiece vibration is accompanied with tool rotation, material straining increases, and higher amount of dislocations are generated; correspondingly, DR intensifies and smaller grains develop [43, 44].

Figure 10 shows the microstructures of various FSSV-welded specimens while different dwelling times (5 and 10 s) and vibration frequencies (28 and 38 Hz) were applied. According to Fig. 10, higher dwell time leads to coarser grains and the grain size decreases as vibration frequency of specimen increases. As dwell time increases, friction between tool and workpiece increases and more heat is produced and this results in grain growth. On the other hand, it is believed that the increase in vibration frequency increases the straining of material and high amount of dislocations are generated. This enhances the DR, and as a result, finer grains develop in the stir zone [45, 46]. Fouladi and Abbasi [45] also found that stir zone grain size during FSVW (friction stir vibration welding) decreases as vibration frequency increases.

The grain size value for base metal as well as stir zone grain sizes of welded specimens for different welding conditions is presented in Fig. 11. It is observed that the grain size values for welded specimens are lower than that for base material and FSSV-welded specimens have smaller grains with respect to FSS-welded specimens. The results are in agreement with observations in microstructural images (Figs. 9, 10).

Tensile Shear Analysis

The tensile shear performance of spot-welded joint is a significant factor in design and manufacturing. The effect
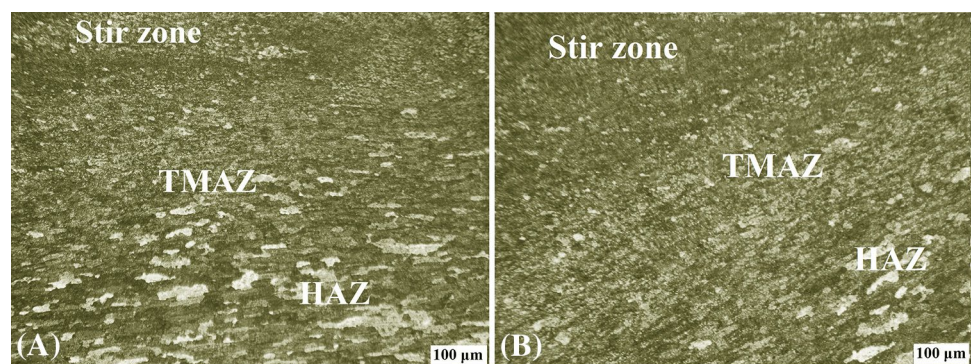
Fig. 7 Cross section of specimens (**a**) FSS- and (**b**) FSSV-welded specimens
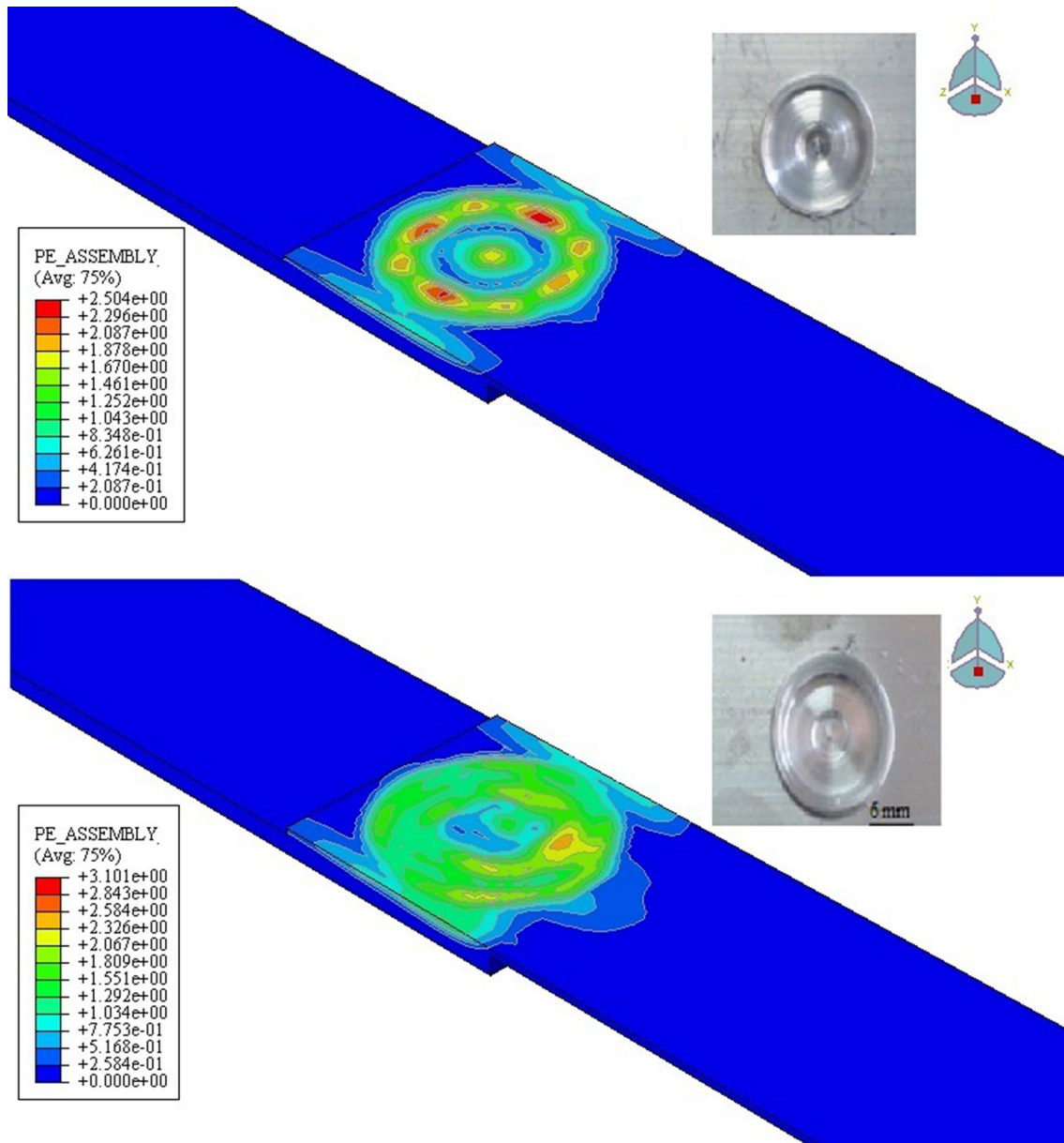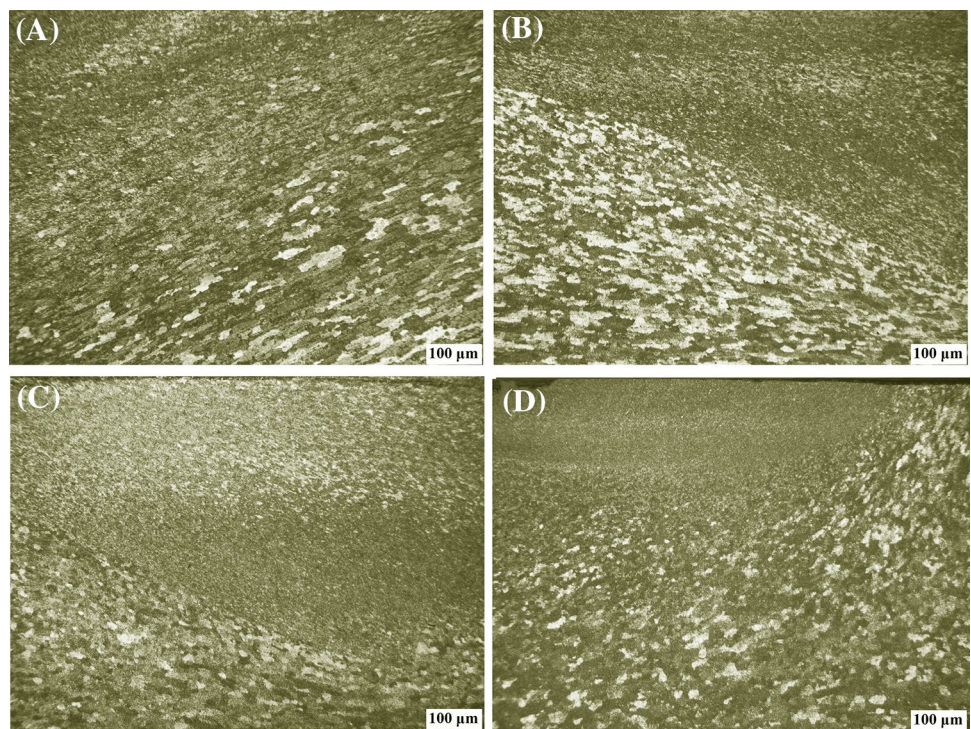
Fig. 8 FE results for strain distribution (**a**) FSS- and (**b**) FSSV-welded specimens

**Fig. 9** Microstructure of welded specimens (**a**) FSS- and (**b**) FSSV-welded specimens

Fig. 10 Microstructures for FSSV-welded specimens using different dwelling times and frequencies (**a**) 28 Hz, 5 s, (**b**) 28 Hz, 10 s, (**c**) 38 Hz, 5 s, and (**d**) 38 Hz, 10 s


Fig. 11 Stir zone grain size values for different welded specimens under various welding conditions; dwell time is indicated in parentheses; and A and B symbols denote the specimens FSSV welded by vibration frequency of 28 Hz and 38 Hz, respectively
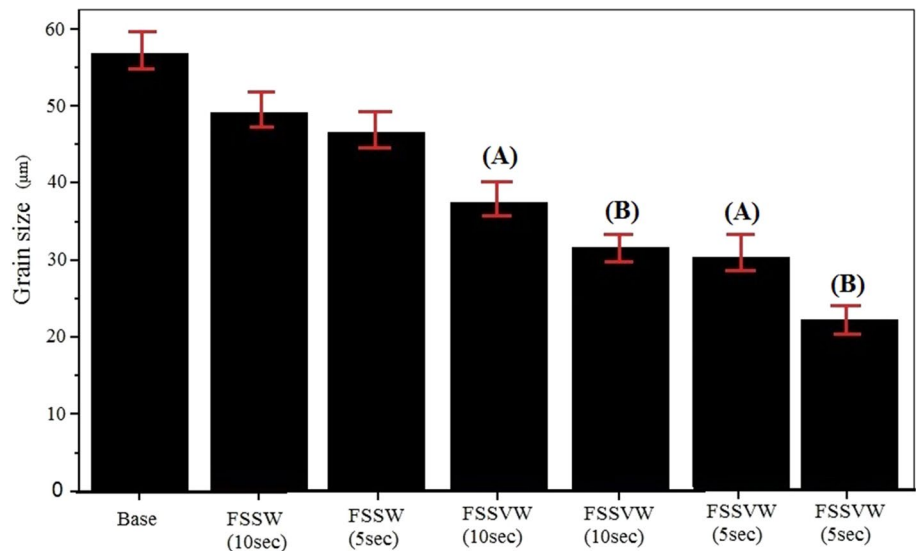

of dwell time and vibration frequency on the tensile shear load of FSS- and FSSV-welded joints is shown in Fig. 12. It is observed in Fig. 12 that shear strength of FSSV-welded specimens is higher than that of FSS-welded ones and strength increases as dwell time decreases and vibration frequency increases. These can be related to the effect of microstructure. As grain size decreases, the volume fraction of grain boundaries increases, and correspondingly, the obstacles for dislocation movement increase.

According to Hall–Petch equation ($\sigma = \sigma0 + kd^{-0.5}$) [48], strength ($\sigma$) increases as grain size (d) decreases. It was observed (Fig. 11) that FSSV-welded specimens had smaller grains than FSS-welded specimens and grain size decreased as vibration frequency increased and dwell time decreased. So, based on Hall–Petch equation, the results in Fig. 12 are predictable. It is also observed in Fig. 12 that for all welding conditions, the simulation results for FSSVW are higher than experimental results. This can
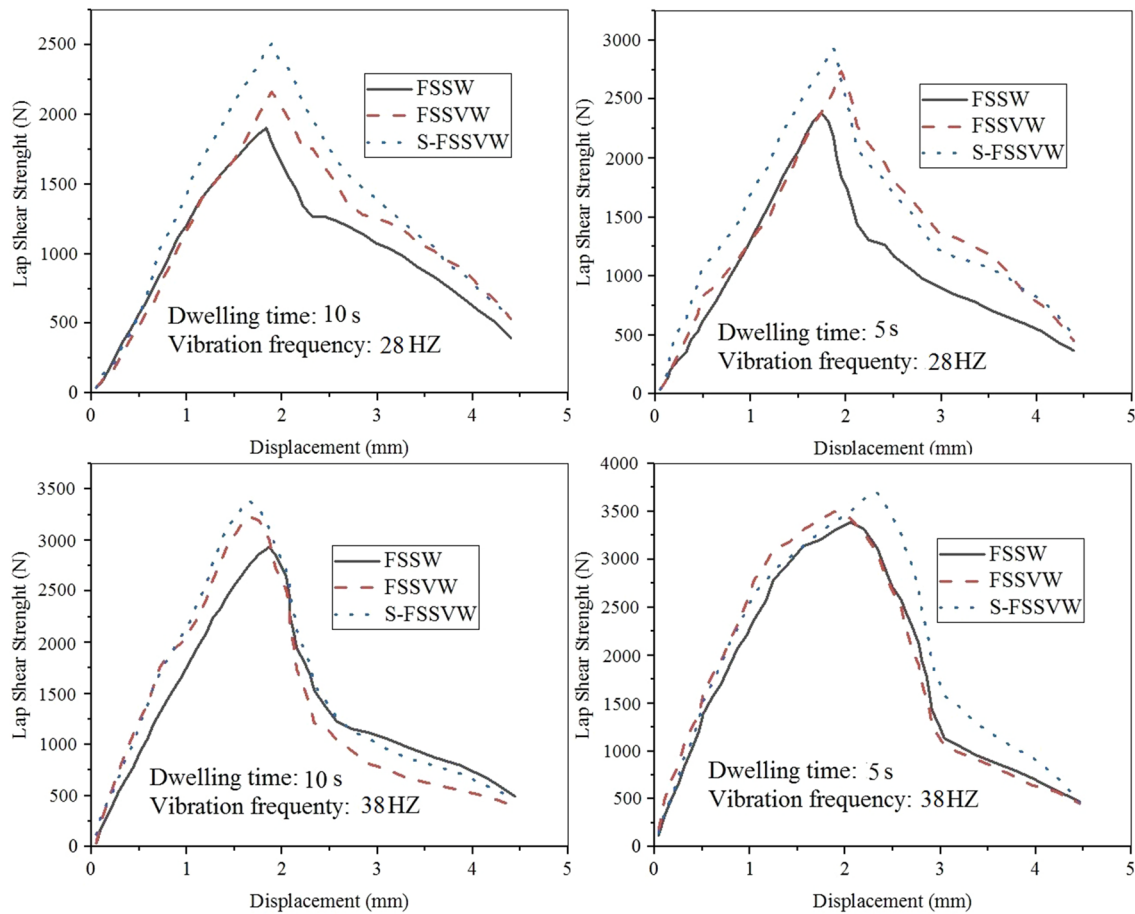
Fig. 12 Effect of dwell time and vibration frequency on the tensile shear strength of FSS- and FSSV-welded specimens. S-FSSVW denotes the simulation result

Fig. 13 Fracture surfaces of (**a**) FSSV-welded specimen in the dwell time of 5 s, and vibration frequency of 28 Hz, (**b**) FSSV-welded specimen in the dwell time of 10 s, and vibration frequency of 28 HZ, (**c**) FSSV-welded specimen in the dwell time of 5 s, and vibration frequency of 38 HZ, and (**d**) FSSV-welded specimen in the dwell time of 10 s, and vibration frequency of 38 Hz
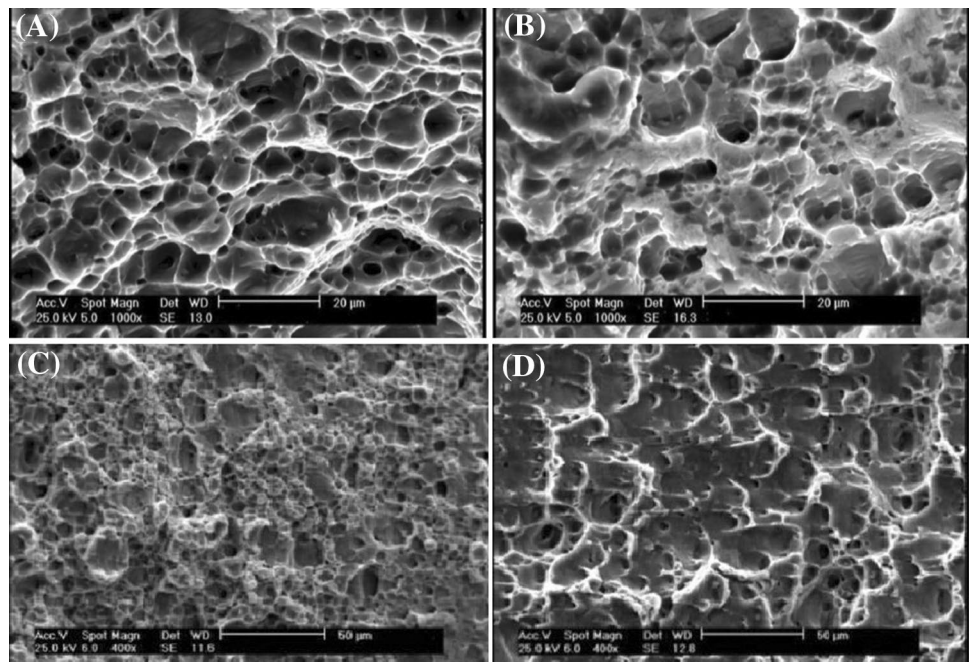
be related to assuming simplifying assumptions during simulation as such stability of friction coefficient during FSSVW results in lower temperature and higher strength.

Fracture Surfaces

Fracture surfaces of FSSV-welded specimens under different welding conditions are presented in Fig. 13. The effects of dwell time and vibration frequency on fracture surfaces are observed in this figure. All specimens show porous surfaces full of dimples. Large plastic deformation and the presence of dimples are characteristics of ductile fracture surfaces [42]. During deformation, dislocations move and their density increases. At early stages of deformation, the dislocations glide freely, but during straining the dislocations intersect with each other and some jogs or barriers are formed [48]. These jogs or barriers are the initial sites for the formation of voids; however, inclusions and secondary phase particles are other preferable sites for void formation [45]. As straining proceeds, voids coalescence and form small cracks which grow, and finally, fracture occurs. The

voids are responsible for the constitution of dimples [45]. It is observed in Fig. 13 that voids size decreases as vibration frequency increases and dwell time decreases. This can be related to the effect of grain size. It is known that voids for metals with fine grains are smaller than those for metals with coarse grains [46, 47]. As vibration frequency increases and dwell time decreases, finer grains develop (Fig. 11), and correspondingly, smaller voids develop.

Hardness

The effect of vibration frequency and dwell time on the hardness of FSSV-welded joints along a path normal to the weld is shown in Fig. 14. Based on Fig. 14, stir zone hardness is higher than other regions and the greatest hardness value belongs to the specimen welded with vibration frequency of 38 Hz and dwell time of 5 s. Figure 14 shows that hardness increases as vibration frequency increases and dwell time decreases. These can be related to the effect of microstructure. It was observed (Fig. 11) that grain size decreased as vibration frequency increased and dwell time decreased. As
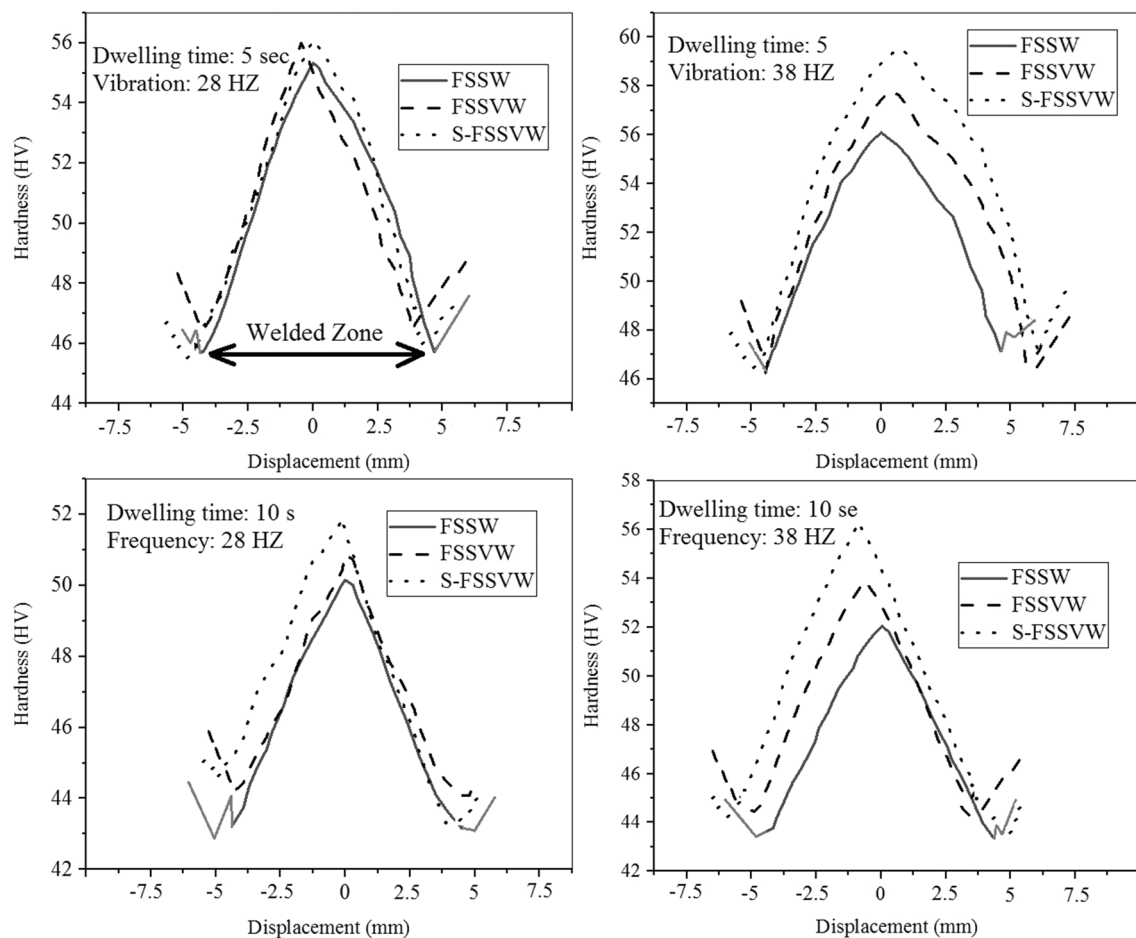

Fig. 14 Hardness distribution along a line passes through the weld region. 0 point coincides with the center of the stir zone

grain size decreases, the volume fraction content of grain boundaries increases. Grain boundaries impede the movement of dislocations, and this increases the hardness [48, 49].

Conclusion

In this study, microstructure and mechanical properties of AA5083 joints made by FSSW and FSSVW processes under different dwell times (5 and 10 s) and vibration frequencies (28 and 38 Hz) were investigated. FSSVW is a modified version of FSSW in which workpiece is vibrated during FSSW and normal to tool axis direction. FSSW and FSSVW processes were also simulated using Abaqus software, and the results were compared with experimental results.

- The results showed that the presence of vibration during FSSW resulted in more grain refinement. The results showed that vibration during FSSW led to grain size decrease of about 35% in the weld region.
- The results indicated that the stir zone microhardness values of FSSV-welded samples were greater than those of FSS-welded samples for about 23%.
- Grain refinement and mechanical properties increased as vibration frequency increased. The tensile shear strength of the joint increased as vibration frequency increased.
- Good agreement was observed between FEM simulation results and experimental results. This indicated that the variable inputs and the assumptions adopted in the FEM model were reasonable.
- It can be concluded that FSSVW, as an inexpensive and easy to apply welding method, is a proper alternative process for FSSW process.

References

1. J.M. Piccini, H.G. Svoboda, Effect of pin length on Friction Stir Spot Welding (FSSW) of dissimilar aluminum-steel joint. Procedia Mater. Sci. **9**, 504–513 (2015)
2. A. Gerlich, P. Su, M. Yamamoto, T.H. North, Effect of welding parameters on the strain rate and microstructure of friction stir spot welded 2024 aluminum alloy. Mater. Sci. **42**, 5589–5601 (2007)
3. J.M. Piccini, H.J. Svoboda, Effect of the tool penetration depth in friction stir spot welding (FSSW) of dissimilar aluminum alloys. Procedia Mater. Sci. **8**, 868–877 (2015)
4. Y. Tozaki, Y. Uematsu, K. Tokaji, Effect of tool geometry on microstructure and static strength in friction stir spot welded aluminium alloys. Mach. Tools Manuf. **47**, 2230–2236 (2007)
5. O. Tuncel, H. Aydin, M. Tutar, A. Bayram, Mechanical performance of friction stir spot welding AA6082-T6 sheets. Mech. Prod. Eng. **4**(1), 114–118 (2016)
6. B. Srinivasulu, Namish Mehta, Friction stir spot welding on similar aluminum alloys Al6082 by using different shape of EN19 and EN31 profile tool. Curr. Eng. Sci. Res. (IJCESR) **4**(10), 8–11 (2017)
7. N. Srirangarajalu, Experimental study on friction stir spot welded aluminium alloy AA 1100. Mech. Eng. Robot. (IJMER) **3**(5), 42–45 (2015)
8. M.K. Kulekci, Effects of process parameters on tensile shear strength of friction stir spot welded aluminium alloy (EN Aw 5005). Arch. Metall. Mater. **59**(1), 221–224 (2014)
9. S.H. Toshiya, M. Kenzo, Y. Shyuhei, Friction stir spot welding of pure aluminum sheet in view of high temperature deformation. Join. Weld. Res. Inst. **40**(2), 1–5 (2011)
10. H. Sheikhhasani, H. Sabet, M. Abbasi, Investigation of the effect of friction stir spot welding of BH galvanized steel plates on process parameters and weld mechanical properties. Eng. Technol. Appl. Sci. Res. **6**(5), 1149–1154 (2016)
11. S.W. Baek, D.H. Choi, ChY Lee, A.S.B. Yeon Jung, Microstructure and mechanical properties of friction stir spot welded galvanized steel. Mater. Trans. **51**(5), 1044–1050 (2010)
12. N. Jafarzadeh Aghdam, S. Hassanifard, M.M. Ettefagh, A. Nanvayesavojblaghi, Investigating fatigue life effects on the vibration properties in friction stir spot welding using experimental and finite element modal analysis. Mech. Eng. **60**(11), 735–774 (2014)
13. A. Dey, S.C. Saha, K.M. Pandey, Study of mechanical properties change during friction stir spot welding of aluminium alloys. Curr. Trends Technol. Sci. Curr. Trends Technol. Sci. **3**(1), 26–33 (2014)
14. C. Schilling, J. Dos Santos, Method and device for linking at least two adjoining pieces by friction welding, US Patent 6722556B2, 2004
15. Y.F. Sun, H. Fujii, N. Takaki, Y. Okitsu, Microstructure and mechanical properties of dissimilar Al alloy/steel joints prepared by a flat spot friction stir welding technique. Mater. Des. **47**, 350–357 (2013)
16. K. Chen, X. Liu, J. Ni, Electrical assisted friction stir spot welding of aluminum alloy to advanced strength steel, in *ASME 2017 12th International Manufacturing Science and Engineering Conference, Los Angeles, California, USA, June 4–8*, 2017
17. Y. Rostamiyan, A. Seidanloo, H. Sohrabpoor, R. Teimouri, Experimental studies on ultrasonically assisted friction stir spot welding of AA6061. Arch. Civ. Mech. Eng. **15**, 335–346 (2015)
18. S.D. Ji, Z.W. Li, Y.M. Yue, S.S. Gao, Investigation of ultrasonic assisted friction stir spot welding of magnesium alloy to aluminum alloy. Strength Mater. **48**, 2–7 (2016)
19. X.C. Liu, C.S. Wu, G.K. Padhy, Characterization of plastic deformation and material flow in ultrasonic vibration enhanced friction stir welding. Scr. Mater. **102**, 95–98 (2015)
20. K. Park, Development and analysis of ultrasonic assisted friction stir welding process. Ph.D Thesis, The University of Michigan, 2009
21. X.C. Liu, C.S. Wu, G.K. Padhy, Improved weld macrosection, microstructure and mechanical properties of 2024Al-T4 butt joints in ultrasonic vibration enhanced friction stir welding. Sci. Technol. Weld. Join. **20**(4), 345–352 (2015)
22. B. Strass, G. Wagner, D. Eifler, Realization of Al/Mg-hybrid-joints by ultrasound supported friction stir welding. Mater. Sci. Forum **783–786**, 1814–1819 (2014)
23. S. Amini, M.R. Amiri, Study of ultrasonic vibrations' effect on friction stir welding. Int. J. Adv. Manuf. Technol. **73**(1–4), 127–135 (2014)
24. M. Ahmadnia, A. Seidanloo, R. Teimouri, Y. Rostamiyan, K.G. Titrashi, Determining influence of ultrasonic-assisted friction stir welding parameters on mechanical and tribological properties of

AA6061 joints. Int. J. Adv. Manuf. Technol. (2015). https://doi.org/10.1007/s00170-015-6784-0

25. Z.H. Liu, S.H. Ji, X. Meng, Joining of magnesium and aluminum alloys via ultrasonic assisted friction stir welding at low temperature. Int. J. Adv. Manuf. Technol. **97**, 4127–4136 (2018)

26. ASTM E3-11, *Standard guide for preparation of metallographic specimens* (ASTM International, West Conshohocken, 2011)

27. ASTM-E112-13, *Standard Test Methods for Determining Average Grain Size* (ASTM International, West Conshohocken, 2013)

28. ABAQUS/6.14.2, Providence, RI, USA: Dassault Systems Simulia Corp, 2016

29. H. Yalavarthy, Friction stir welding process and material microstructure evolution modeling in 2000 and 5000 series of aluminum alloys. All Thesis, Clemson university, 2009

30. M.Z.H. Khandkar, J.A. Khan, A.P. Reynolds, Prediction of temperature distribution and thermal history during friction stir welding: input torque based model. Sci Technol. Weld. Join. **8**(3), 165–174 (2003)

31. J.W. Pew, T.W. Nelson, C.D. Sorenson, Torque based weld power model for friction stir welding. Sci. Technol. Weld. Join. **12**, 341–347 (2007)

32. M. Mijajlovic, D. Milcic, Analytical model for estimating the amount of heat generated during friction stir welding: application of plates made of aluminum alloy 2024 T351, *Welding processes*, Chap. 11 (InTech, 2012), pp. 247–274

33. P. Ferro, F. Bonollo, A semianalytical thermal model for friction stir welding. Metall. Mater. Trans. A **41**, 440–449 (2009)

34. H. Atharifar, D. Lin, R. Kovacevic, Numerical and experimental investigations on the loads carried by the tool during friction stir welding. J. Mater. Eng. Perform. **18**, 339–350 (2008)

35. H. Schmidt, J. Hattel, J. Wert, An analytical model for heat generation in friction stir welding. Modell. Simul. Mater. Sci. Eng. **12**, 143–157 (2004)

36. D.H. Lammlein, D.R. DeLapp, P.A. Fleming, A.M. Strauss, G.E. Cook, The application of shoulderless conical tools in friction stir welding: an experimental and theoretical study. Mater. Des. **30**, 4012–4022 (2009)

37. R. Nandan, T. DeBroy, Numerical simulation of three-dimensional heat transfer and plastic flow during friction stir welding. Metall. Mater. Trans. A **37**, 1247–1259 (2006)

38. Y. Huang, Y. Wang, X. Meng, L. Wan, J. Cao, L. Zhou, J. Feng, Dynamic recrystallization and mechanical properties of friction stir processed Mg-Zn-Y-Zr alloys. J. Mater. Process.

Technol. **249**, 331–338 (2017). https://doi.org/10.1016/j.jmatprotec.2017.06.021. **(Accepted Manuscript)**

39. A.G. Rao, K.R. Ravi, B. Ramakrishnarao, V.P. Deshmukh, A. Sharma, N. Prabhu, B.P. Kashyap, Recrystallization phenomena during friction stir processing of hypereutectic aluminum-silicon alloy. Metall. Mater. Trans. A **44**, 1519–1529 (2013)

40. M. Rahmi, M. Abbasi, Friction stir vibration welding process: modified version of friction stir welding process. Int. J. Adv. Manuf. Technol. **90**, 141–151 (2017)

41. S. Fouladi, A.H. Ghasemi, M. Abbasi, M. Abedini, A.M. Khorasani, I. Gibson, The effect of vibration during friction stir welding on corrosion behavior. Mech. Prop. Mach. Charact. Stir Zone Met. **7**, 421–435 (2017)

42. W.D. Callister, *Materials Science and Engineering: An Introduction* (Wiley, USA, 2007)

43. K.V. Jata, S.L. Semiatin, Continuous dynamic recrystallization during friction stir welding of high strength aluminum alloys. Scr. Mater. **43**, 743–749 (2000)

44. J.Q. Su, T.W. Nelson, C.J. Sterling, Microstructure evolution during FSW/FSP of high strength aluminum alloys. Mater. Sci. Eng. A **405**, 277–286 (2005)

45. S. Fouladi, M. Abbasi, The effect of friction stir vibration welding process on characteristics of SiO2 incorporated joint. J. Mater. Process. Technol. **243**, 23–30 (2017)

46. B. Bagheri, M. Abbasi, M. Givi, Effects of vibration on microstructure and thermal properties of friction stir spot welded (FSSW) aluminum alloy (Al5083). Int. J. Precis. Eng. Manuf. (2019). https://doi.org/10.1007/s12541-019-00134-9

47. M. Abbasi, M. Givi, B. Bagheri, Application of vibration to enhance the efficiency of friction stir processing. J. Trans. Nonferrous Met. Soc. China **29**, 1393–1400 (2019)

48. D. Hull, D.J. Bacon, *Introduction to Dislocations* (Butterworth-Heinemann, Britain, 2011), pp. 87–95

49. B. Bagheri, M. Abbasi, Analysis of microstructure and mechanical properties of friction stir vibration welded (FSVW) 5083 aluminum alloy joints: experimental and simulation. J. Weld. Join. (2019). https://doi.org/10.5781/jwj.2019.37.3.82019